Optical Materials 174 (2026) 117921

Contents lists available at ScienceDirect

Optical Materials

journal homepage: www.elsevier.com/locate/optmat

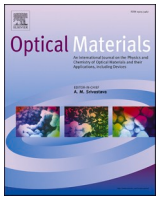

Research Article

Tailoring the first hyperpolarizability of acetamide-chalcone derivatives

André G. Pelosi [a], João V.P. Valverde [a], Carlos H. dos Santos [a], EliS.A. Ducas [b], Pablo J. Gonçalves [b,c], Cleber Renato Mendonça [a], Leonardo De Boni [a,*]

[a] São Carlos Institute of Physics, University of São Paulo, CP 369, São Carlos, SP, 13560-970, Brazil
[b] Instituto de Química, Universidade Federal de Goiás, Goiânia, GO, 74690-900, Brazil
[c] Instituto of Physics, Federal University of Goiás, Goiânia, GO, 74690-900, Brazil

ARTICLE INFO

Keywords:
Acetamide-chalcones
First-order molecular hyperpolarizability
Hyper-Rayleigh scattering
Second-harmonic generation
N-level model
Nonlinear optical effect
Femtosecond lasers

ABSTRACT

We employed the femtosecond laser-induced Hyper-Rayleigh Scattering technique to measure the dispersion of the first-order molecular hyperpolarizability (β) of five acetamide-chalcone derivatives containing different electron-donating groups. Our results show that β strongly depends on the excitation wavelength, exhibiting an approximately sevenfold increase at 750 nm compared to the static value, β_s. We demonstrated that this effect is the result of two-photon resonance enhancement. We also observed that the β dispersion increases with the electron-donating strength of the substituents, reflecting the intensification of intramolecular charge transfer (ICT) along the π-conjugated system. Both β and the two-photon absorption (2 PA) cross-section show a linear increase with the Hammett constant, reinforcing the central role of ICT in the nonlinear optical response. Furthermore, we employed a phenomenological *n*-level model (*n*LM) to fit the experimental β dispersion and compared it with the well-known Sum-Over-States model for 2 PA. Both models showed good agreement, resulting in similar photophysical parameters, demonstrating the consistency of the adopted treatment. Thus, this work elucidates an efficient mechanism for optimizing β in acetamide-chalcone derivatives, combining appropriate molecular functionalization with the selection of the excitation spectral region.

1. Introduction

The recent interest in new organic materials with high first-order molecular hyperpolarizability (β) stems from their potential use as probes based on incoherent second-harmonic generation (ISHG) in biological systems, enabling safe, non-invasive, and high-spatial-resolution optical imaging, both *in vivo* and *in vitro* [1–5]. This relevance is associated with the unique characteristics of the ISHG process. Due to its quadratic dependence on the excitation beam intensity [6] and the use of light typically in the near-infrared region (NIR-I: 700–900 *nm* and NIR-II: 1000 – 2000 *nm*) [2], ISHG offers high spatial confinement and deeper penetration in biological tissues [7]. These features enable imaging with high optical sectioning capability in thick and complex samples while simultaneously reducing light linear scattering [1,7]. ISHG microscopy and two-photon excited fluorescence microscopy share several technical similarities; however, ISHG presents significant advantages, including instantaneous response, absence of photobleaching, independence from the laser repetition rate, and high selectivity [1,8,9].

ISHG microscopy minimizes photodamage effects by employing excitation outside the resonance region. However, as it is a nonlinear process that requires high excitation intensities, other photodamage mechanisms may still occur. Thus, a central concern in all forms of nonlinear imaging is to optimize sensitivity while avoiding undesirable effects [2]. In this context, designing highly efficient organic compounds becomes essential so that ISHG can occur under the lowest possible excitation powers. Several molecular design strategies have been proposed and have proven promising in different fields of nonlinear photonics [10–16]. In general, these strategies involve extending the π-conjugated system and functionalizing the molecular framework with lateral groups that can donate or withdraw electrons. This type of molecular architecture is commonly represented as X–π–X, where X can act as either an electron-donating or electron-withdrawing (ED and EW, respectively) group, giving rise to structures of the type ED–π–ED, ED–π–EW, and EW–π–EW, in which the donating and withdrawing strengths play a fundamental role in the magnitude of β [10,11,17–22]. Furthermore, other more complex architectures, such as branched molecules [22,23] and organic crystals [13,24], have also exhibited high

* Corresponding author.
E-mail address: deboni@ifsc.usp.br (L. De Boni).

https://doi.org/10.1016/j.optmat.2026.117921
Received 29 November 2025; Received in revised form 20 January 2026; Accepted 25 January 2026
Available online 26 January 2026

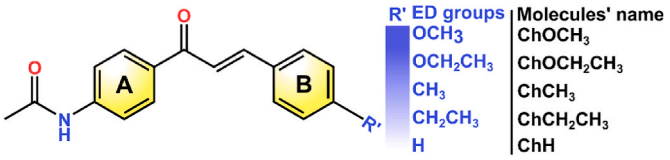

Fig. 1. – Molecular structure of the acetamide-chalcone derivatives, where R′ denotes the position of the electron-donating groups: –H, $–CH_2CH_3$, –CH3, $–OCH_2CH_3$, and $–OCH_3$.

β values.

In addition to molecular design, the efficiency of ISHG also strongly depends on the excitation conditions. The choice of an appropriate spectral region is crucial for maximizing the β values. Hall et al. [25] demonstrated that for longer excitation wavelengths, the ISHG intensity decreases sharply, dropping by more than one order of magnitude between 780 *nm* and 1230 *nm*. They also showed that although longer wavelengths provide greater penetration depth, this effect does not compensate for the reduction in β. Santos et al. [18] also observed that, in organic molecules with ED–π–EW structure, β exhibits a pronounced increase in spectral regions close to two-photon transitions, highlighting another important mechanism for enhancing ISHG. However, most studies on the measurement of β are performed at a fixed excitation wavelength, usually employing the hyper-Rayleigh scattering (HRS) technique [21,23,26,27]. Therefore, in addition to designing molecules with high β, it is equally important to identify the optimal excitation spectral ranges to fully explore the potential of these materials.

Chalcones and their derivatives represent a promising class of materials. Chalcones belong to an abundant group of natural substances known as flavonoids and isoflavonoids, characterized by an α,β-unsaturated carbonyl group that connects two aromatic rings [28–30]. This structure exhibits remarkable features: a straightforward synthetic route, generally good biocompatibility, low intrinsic toxicity, and ease of functionalization of the main framework with ED or EW substituents [31–36]. Such structural modifications can substantially alter the photophysical properties of the molecule, enabling the design of molecules with application-oriented properties. For instance, functionalization with the acetamide group has been associated with relevant bioactive properties, broadening the potential of these derivatives in biological contexts [33,37–39]. Moreover, certain lateral groups can induce the formation of highly emissive states, allowing the use of chalcone derivatives as fluorescent bioprobes [35,36,40]. Nevertheless, a significant fraction of these molecules remains weakly fluorescent or, in most cases, non-fluorescent [18,19,31,41,42]. This intrinsic non-emissive character makes chalcones particularly attractive for ISHG-based bioimaging techniques, as several studies have demonstrated that this class of materials constitutes a promising platform for nonlinear-optics applications [18,19,43–45].

In this context, we investigated how the functionalization of acetamide-chalcone with five different ED groups modulates the spectral dispersion of β. These compounds exhibit an ED–π–ED architecture, whose lateral groups display a progressive increase in electron-donating strength: $–H < –CH_2CH_3 < –CH_3 < –OCH_2CH_3 < –OCH_3$. This design meets the criteria established in the literature for molecules displaying remarkable nonlinear optical response [10,11,17–22]. In this contribution, we determined the spectral dispersion of β in the $750 - 1100\ nm$ range using the femtosecond laser-induced HRS technique and applied the *n*-level model (*n*LM) to elucidate the ISHG mechanism. In a recent study [46], we determined the linear photophysical properties and the two-photon absorption (2 PA) process of these same compounds, complementing the experimental results with quantum chemical calculations (QCCs) and with the Sum-Over-States (SOS) model. We demonstrated that the different lateral groups exert a strong influence on the 2 PA process. Altogether, these findings indicate that this family of molecules constitutes a promising platform for investigating and tailoring β.

2. Materials and methods

2.1. Samples

We studied five acetamide-chalcone derivatives with an ED-π-ED molecular architecture, as shown in Fig. 1. The compounds were synthesized via a base-catalyzed Claisen-Schmidt condensation between 4′-acetoamidoacetophenone (ring A) and substituted benzaldehydes (ring B), affording the target compounds in moderate yields (∼ 46%). The detailed synthesis and structural characterization are reported in Ref. [46]. All compounds feature an acetamide group attached to ring A and different ED groups ($–CH_2CH_3$, $–CH_3$, $–OCH_2CH_3$, $–OCH_3$, and unsubstituted) bonded to ring B. We named the compounds according to the substituent group: **ChH** *(N-[4-[(2E)-1-oxo-3-phenyl-2-propen*-1-yl*]phenyl]acetamide)*, **ChCH$_3$** *(N-[4-[(2E)-3-(4-methylphenyl)-1-oxo-2-propen*-1-yl*]phenyl]acetamide)*, **ChCH$_2$CH$_3$** *(N-[4-[(2E)-3-(4-ethylphenyl)-1-oxo-2-propen*-1-yl*]phenyl]acetamide)*, **ChOCH$_3$** *(N-[4-[(2E)-3-(4-methoxyphenyl)-1-oxo-2-propen*-1-yl*]phenyl]acetamide)*, and **ChOCH$_2$CH$_3$** *(N-[4-[(2E)-3-(4-ethoxyphenyl)-1-oxo-2-propen*-1-yl*]phenyl]acetamide)*.

2.2. Linear measurements

For the one-photon absorption (1 PA) measurements, we dissolved the acetamide-chalcone derivatives in pure dimethylsulfoxide (DMSO –

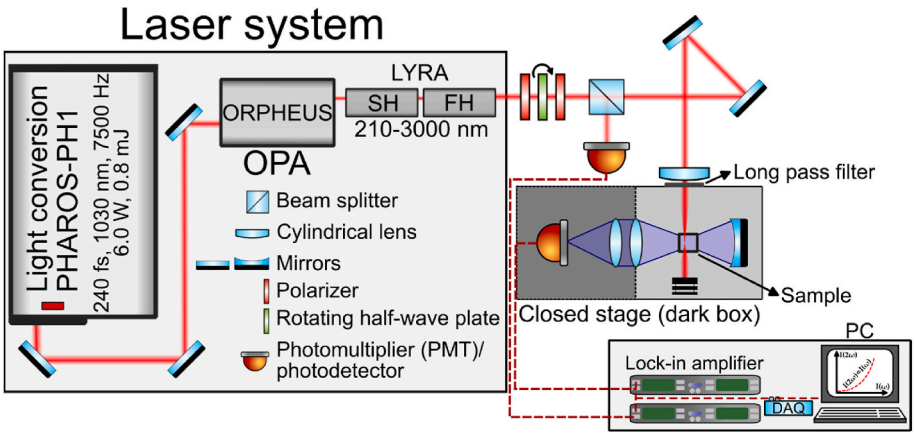

Fig. 2. – Schematic representation of the femtosecond laser-induced hyper-Rayleigh scattering (HRS) technique used for the determination of the first-order molecular hyperpolarizability (β).

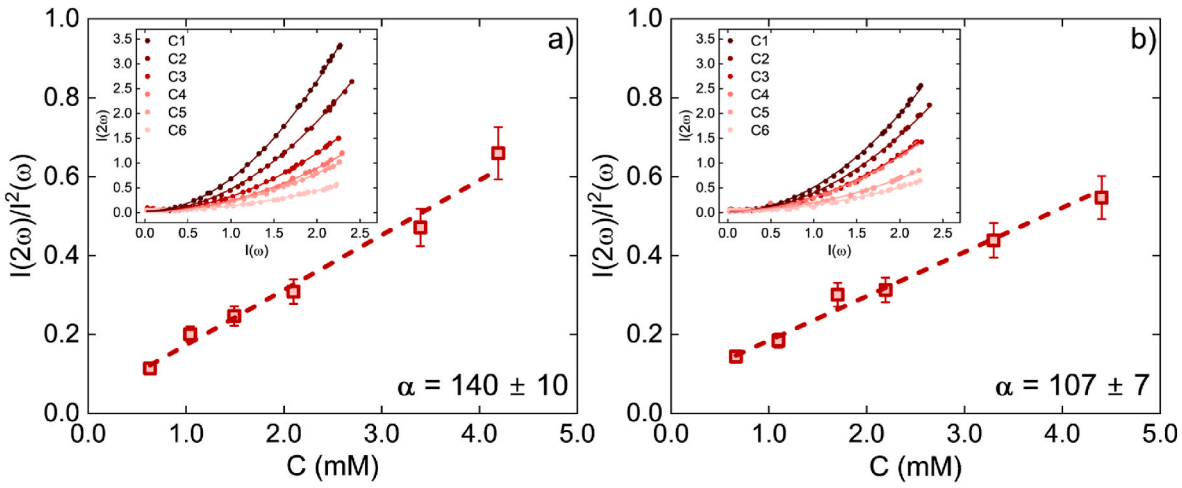

Fig. 3. – Ratio between the second harmonic scattering signal and the square of the incident beam intensity $[I(2\omega)/I^2(\omega)]$, as a function of concentration C, at 750 nm (red squares) for: a) **Ch** and b) *para*-nitroaniline (pNA), both in DMSO. The red dashed line represents the linear fit, and the corresponding slopes (α). The inset displays the $I(2\omega)$ *versus* $I(\omega)$ (red circles) for different concentrations C_i (for $i = 1, 2, 3, 4, 5,$ and 6). (For interpretation of the references to colour in this figure legend, the reader is referred to the Web version of this article.)

P.A), a solvent in which the compounds exhibit high solubility, at concentrations on the order of 1×10^{-4} *mol·L*$^{-1}$. We placed the solutions in fused silica cells with an optical path length of 2 *mm*. We obtained the 1 PA spectra using a UV–Vis spectrometer (UV-1800, Shimadzu) and did not observe aggregate formation. Additionally, the compounds exhibited no fluorescence emission, as verified using a spectrofluorometer (F-7000, Hitachi), as also reported in a previous study [46].

2.3. Tunable femtosecond HRS technique

We determined the spectral dispersion of β using a femtosecond laser-induced HRS technique, as described in Ref. [18]. The experimental setup is based on a regeneratively amplified Yb:KGW femtosecond laser system (Pharos PH1, Light Conversion), operating at a central wavelength of 1030 *nm*, with a pulse duration of $\sim$ 240 fs, a repetition rate of 7.5 *kHz*, and a pulse energy of 0.8 *mJ*. This system laser pumps an optical parametric amplifier (OPA; Orpheus, Light Conversion), which delivers tunable excitation wavelengths from 220 to 3000 *nm* with pulse durations of 100 − 180 fs.

Fig. 2 presents a schematic figure of the experimental setup. Briefly, the HRS technique consists of monitoring, for each pump frequency ω, the second harmonic scattering signal $[I(2\omega)]$as a function of the incident beam intensity $[I(\omega)]$. To this end, we employed two polarizers in combination with a rotating broadband half-wave plate, allowing precise control of the OPA-generated beam intensity while maintaining vertical polarization. A beam splitter directs a small fraction of the pump beam ($\sim$ 4%) to a reference photodetector (silicon or germanium). The main portion of the beam ($\sim$ 96%) is focused onto the sample using a cylindrical lens, thereby increasing the irradiated area and, consequently, the number of scattering centers. The HRS signal is collected at 90° with respect to the pump beam and directed to a photomultiplier (PMT) via a lens-telescope and a concave spherical mirror, with the entire detection system housed in a dark box. At the entrance to the PMT, we placed appropriate short-wave pass filters to eliminate possible scattering from the pump beam. Both the PMT and the reference photodetector are connected to lock-in amplifiers, which are triggered at the laser repetition rate. The insets of Fig. 3 show typical curves of $I(2\omega)$ *versus* $I(\omega)$, highlighting the quadratic behavior, as expected [17,47,48].

We calculated the β magnitude using the External Reference Method (ERM), as described in Refs. [31,47,49–51]. Briefly, this method relies on a standard molecule whose β values are well known. To this end, we performed measurements of $I(2\omega)$ as a function of $I(\omega)$ for different concentrations of both the standard and the investigated samples. In the case of HRS, the ratio $I(2\omega)/I^2(\omega)$ exhibits a linear dependence on the concentration, as illustrated in Fig. 3. Thus, by performing a linear regression of the $I(2\omega)/I^2(\omega)$ curves as a function of concentration for the standard and the investigated samples, we obtain the slopes ($\alpha_{standard}$ and α_{sample}), from which the β magnitude can be determined according to [18,52]

$$\beta_{sample} = \beta_{standard}\sqrt{\frac{\alpha_{sample}}{\alpha_{standard}}}. \quad (1)$$

It is worth noting that Eq. (1) is valid provided that the same solvent and identical experimental parameters are used for both the standard and the investigated samples [18]. In this work, we used *para*-nitroaniline (pNA) as a standard sample, whose β values were obtained from the work of Sciuti et al. [41]. For the HRS measurements, we prepared six solutions of the acetamide-chalcone derivatives and pNA in DMSO, with concentrations ranging from 1×10^{-4} to 1×10^{-3} *mol·L*$^{-1}$. We placed the solutions in fused silica cells with an optical path length of 10 *mm*. Finally, we performed the measurements in the 750 − 1100 *nm* spectral range with 50 *nm* increments.

3. Results and discussions

Fig. 4 presents the 1 PA spectra (solid blue lines) for all acetamide-chalcone derivatives in DMSO. As can be observed, the compounds exhibit a broad absorption band in the spectral range from 275 to 425 *nm*. In a previous work [46], we demonstrated, through Gaussian decomposition, QCCs, and 2 PA spectroscopy, that this band is composed of two energetically close electronic transitions. These transitions are centered at *ca.* 317 *nm* and 346 *nm*, with molar absorptivity (ε) of about 1.3×10^4 $M^{-1}cm^{-1}$ and 3.2×10^4 $M^{-1}cm^{-1}$, respectively. For wavelengths longer than 425 *nm*, all compounds are optically transparent, ensuring the absence of 1 PA in the spectral region where the HRS measurements were performed. As previously discussed, we observed no fluorescence emission for any of the compounds. These results are important for a better understanding of β dispersion data, as discussed below. Further details about these measurements and calculations can be found in Ref. [46].

As shown in Fig. 4 (red circles), the spectral dispersion of β for all compounds in DMSO exhibits a strong dependence on the pump wavelength (λ^{pump}). For discussion purposes, we can divide the spectrum into two regions. In the 900 − 1100 *nm* region, the dispersion of β shows only slight variations, indicating a tendency toward a constant value. This

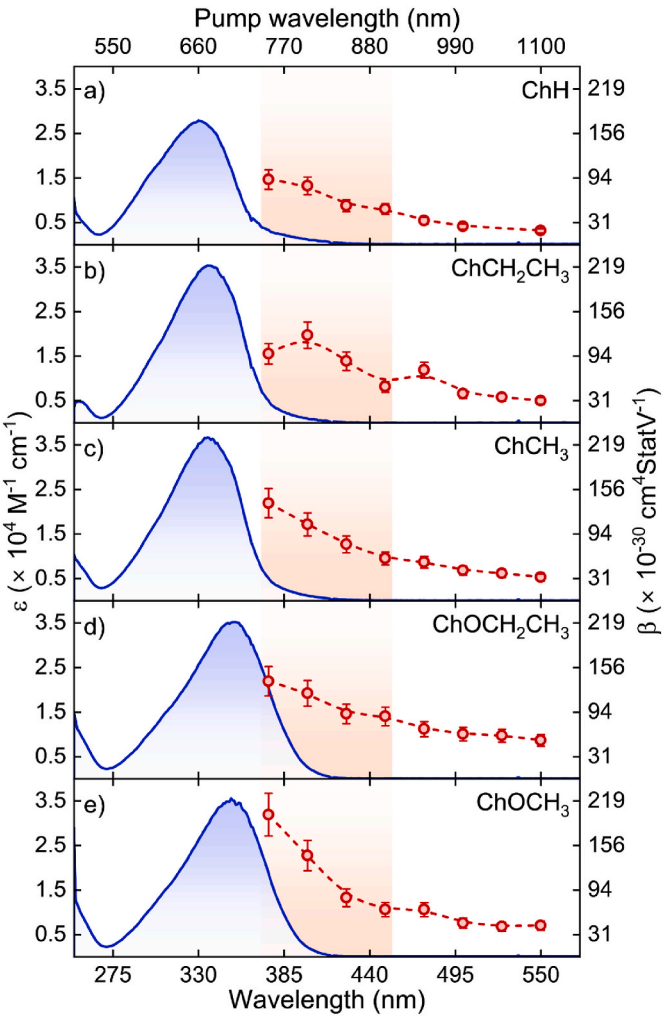

Fig. 4. – One-photon absorption (blue lines: left and bottom axes) and first-order molecular hyperpolarizability dispersion (β) spectra (red circles: right and top axes) for: a) **ChH**, b) **$ChCH_2CH_3$**, c) **$ChCH_3$**, d) **$ChOCH_2CH_3$**, and e) **$ChOCH_3$** in DMSO. The top axis corresponds to the pump wavelength λ^{Pump}. The dashed red lines serve as a guide to the eye. (For interpretation of the references to colour in this figure legend, the reader is referred to the Web version of this article.)

Table 1
– Parameters of the first-order molecular hyperpolarizability for the acetamide-chalcone derivatives in DMSO, including β measured at 750 *nm*, $\beta_\circ$, and their ratio $\beta^* = \beta(750)/\beta_\circ$.

Compound	$\beta(750)$ $(\times 10^{-30} cm^4 statV^{-1})$	$\beta_\circ$ $(\times 10^{-30} cm^4 statV^{-1})^\dagger$	β^*
ChH	90 ± 10	12 ± 2	8 ± 2
$ChCH_2CH_3$	100 ± 20	19 ± 3	5 ± 1
$ChCH_3$	160 ± 10	22 ± 3	7 ± 2
$ChOCH_2CH_3$	140 ± 20	21 ± 3	6 ± 1
$ChOCH_3$	200 ± 30	28 ± 4	7 ± 2

† The values of β_0 were estimated according to Refs. [18,41]: $\beta_0 = \frac{3}{2}\frac{\Delta\mu_{01}\mu_{01}^2}{(\hbar\omega_{01})^2} + \frac{3}{2}\frac{\Delta\mu_{02}\mu_{02}^2}{(\hbar\omega_{02})^2} + \frac{3}{2}\frac{\mu_{01}\mu_{02}\mu_{12}}{\hbar\omega_{01}\hbar\omega_{02}}$, and the parameters were extracted from Ref. [46].

behavior is likely associated with the proximity to the static first-order molecular hyperpolarizability ($\beta_\circ$) region, whose estimated values are summarized in Table 1. In contrast, at shorter wavelengths (< 900 *nm*), the dispersion is characterized by a significant increase in the magnitude

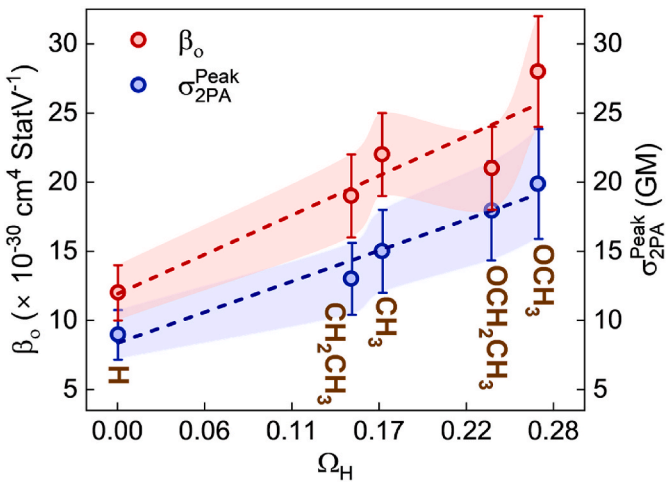

Fig. 5. – Static first-order molecular hyperpolarizability ($\beta_\circ$) and peak two-photon absorption cross-section (σ_{2PA}^{Peak}) values as a function of the Hammett constant (Ω^H) (substituents: –H, $–CH_2CH_3$, $–CH_3$, $–OCH_2CH_3$, and $–OCH_3$). The σ_{2PA}^{Peak} values were extracted from Ref. [46].

of β as λ^{pump} approaches the lowest-energy electronic transition. Within the investigated spectral range, the highest β values are obtained at 750 *nm* (see Table 1), being approximately seven times larger on average than $\beta_\circ$ values.

The enhancement of β observed in the 750 – 900 *nm* spectral window indicates that the ISHG process is mediated by a two-photon allowed transition. In a previous study [46], we demonstrated that, within this range, the compounds indeed exhibit a two-photon-allowed state with an appreciable 2 PA cross-section (σ_{2PA}), reaching average values of approximately 6 *GM* at 750 *nm*. Moreover, Santos et al. [18] and Sciuti et al. [19], in studies involving compounds structurally similar to chalcones, also observed that the ISHG is intensified by 2 PA, thus supporting this assumption. A more detailed analysis of the origin of this effect, based on the *n*LM, is presented below.

The observation of a non-zero β indicates that the investigated acetamide-chalcone derivatives exhibit a low charge symmetry [17,18]. Although the general architecture of these compounds is of the ED–π–ED type, this asymmetry arises from an electronic imbalance between the two sides of the molecule (as evidenced by the molecular orbitals in Ref. [46]), resulting from the different electron-donating strengths of the peripheral groups. This low charge symmetry is also manifested in other molecular properties, leading to a non-zero difference between the permanent dipole moments of the ground and excited states (see Table SI1) and rendering one-photon-allowed states accessible via 2 PA, as previously observed [46].

Assuming the **ChH** molecule as a reference, we can observe that the β values increase with the electron-donating strength of the substituents. For instance, the β dispersion of the **$ChOCH_3$** molecule is about 2-fold larger than observed for the reference one. This behavior can be attributed to the enhancement of intramolecular charge transfer (ICT) along the π-conjugated system, promoted by the ED groups, resulting in increased efficiency in the ISHG process [10,17]. Indeed, in a previous study [46], we observed, through analysis of molecular orbitals, that the **$ChOCH_3$** and **$ChOCH_2CH_3$** molecules exhibit a more pronounced charge transfer upon excitation from the highest occupied to the lowest unoccupied molecular orbitals than the **ChH**, **$ChCH_3$** and **$ChCH_2CH_3$** molecules. Fig. 5 highlights this relationship, showing that the peak values of 2 PA cross-section (σ_{2PA}^{Peak}), previously reported in Ref. [46], and $\beta_\circ$ increase linearly with the Hammett constant (Ω^H) [53]. This correlation suggests that the mechanisms responsible for the nonlinear optical response, both second- and third-order, are strongly dependent on the ICT process.

Table 2
– Values of the transition dipole moment between the first and second excited states (μ_{12}) obtained from the *n*-level model (*n*LM) fit to the first-order molecular hyperpolarizability dispersion (μ_{12}^{nLM}) and from the Sum-Over-States (SOS) model applied to the 2 PA spectrum (μ_{12}^{SOS}). The μ_{12}^{SOS} values were extracted from Ref. [46].

Compound	μ_{12}^{nLM} (D)	μ_{12}^{SOS} (D)
ChH	6.0 ± 1.0	6.1 ± 0.2
$ChCH_2CH_3$	4.0 ± 1.0	4.2 ± 0.2
$ChCH_3$	4.5 ± 0.7	4.0 ± 0.3
$ChOCH_2CH_3$	7.5 ± 0.9	7.3 ± 0.2
$ChOCH_3$	3.0 ± 0.7	2.6 ± 0.3

All the observations presented above indicate that the OCH_3 group plays a key role in enhancing the β values. This influence has also been noted in other studies [54–56]. Abegão et al. [45,57] observed that chalcone derivatives functionalized with OCH_3 groups exhibit higher $\beta_{\circ}$ values. Following the same trend, Muhammed et al. [20] reported an increase in $\beta_{\circ}$ from 24×10^{-30} to 76×10^{-30} cm^4 $stat$ V^{-1} in compounds structurally similar to those investigated in this work. In addition to the enhancement of β associated with the presence of the OCH_3 group, we also showed that the **$ChOCH_3$** molecule exhibited the highest σ_{2PA} values within the series of compounds investigated [46], indicating that, for our chalcone derivatives, strong electron-donating groups play an important role in enhancing the nonlinear optical response.

To gain a better understanding of the behavior of β dispersion, we applied the *n*LM to the experimental results [18,58], considering a three-level system (one ground state and two excited states: 3LM). This model is expressed as follows [18,31,58]:

$$\beta_{3LM} = \beta_{2LM} + \left\{ \left[\frac{3}{2}\frac{\mu_{01}\mu_{02}\mu_{12}}{(\hbar\omega_{01})(\hbar\omega_{02})}\right] \left[\left(\frac{1}{3}\frac{\omega_{01}}{[(\omega_{01}-2\omega)-i\Upsilon_{01}]}\frac{\omega_{02}}{[(\omega_{02}-\omega)-i\Upsilon_{02}]}\right) + \left(\frac{1}{3}\frac{\omega_{02}}{[(\omega_{02}-2\omega)-i\Upsilon_{02}]}\frac{\omega_{01}}{[(\omega_{01}-\omega)-i\Upsilon_{01}]}\right) \right] + \left[\frac{3}{2}\frac{\mu_{02}^2\Delta\mu_{02}}{(\hbar\omega_{02})^2}\right] \left[\left(\frac{1}{3}\frac{\omega_{02}}{[(\omega_{02}-2\omega)-i\Upsilon_{02}]}\frac{\omega_{02}}{[(\omega_{02}-\omega)-i\Upsilon_{02}]}\right) \right] \right\} = B_{11}+B_{12}+B_{21}+B_{22}. \quad (2)$$

Where μ_{0i} represents the transition dipole moment from the ground state to the *i-th* excited one ($i = 1$ and 2), μ_{12} corresponds to the transition dipole moment between the first and second excited states, and $\Delta\mu_{0i} = \mu_{ii} - \mu_{00}$ is the difference between the permanent dipole moments of the ground and *i-th* excited states. ω is the angular frequency of the incident light, while ω_{0i} and Υ_{0i} represent, respectively, the angular frequency and the bandwidth associated with the *i-th* excited state. Finally, the term describing a two-level system, β_{2LM} (one ground state and one excited state: 2LM), is given by Refs. [17,18,41,58]:

$$\beta_{2LM} = \left[\frac{3\mu_{01}{}^2\Delta\mu_{01}}{2(\hbar\omega_{01})^2}\right] \left[\left(\frac{1}{3}\frac{\omega_{01}}{[(\omega_{01}-\omega)-i\Upsilon_{01}]}\frac{\omega_{01}}{[(\omega_{01}-2\omega)-i\Upsilon_{01}]}\right) \right]. \quad (3)$$

In Eqs. (2) and (3), the terms within the square brackets, which are ω-independent, define $\beta_{\circ}$ (as previously presented), whereas the remaining ω-dependent terms define the dynamic β [17,41].

Therefore, to apply the *n*LM (Eq. (2)), we previously determined the parameters μ_{0i} and ω_{0i} through Gaussian decomposition of the compounds' 1 PA spectra in DMSO, using a bandwidth of $\Upsilon \approx 0.2 - 0.3$ eV. In addition, we obtained the $\Delta\mu_{0i}$ values from QCCs at the TD-CAM-B3LYP/6-311++G (d,p) level, employing a polarizable continuum model to account for the DMSO solvent. All these parameters are reported in Ref. [46] and summarized in Table SI1. Consequently, the only free parameter during the fitting of 3LM to the experimental data is μ_{12}.

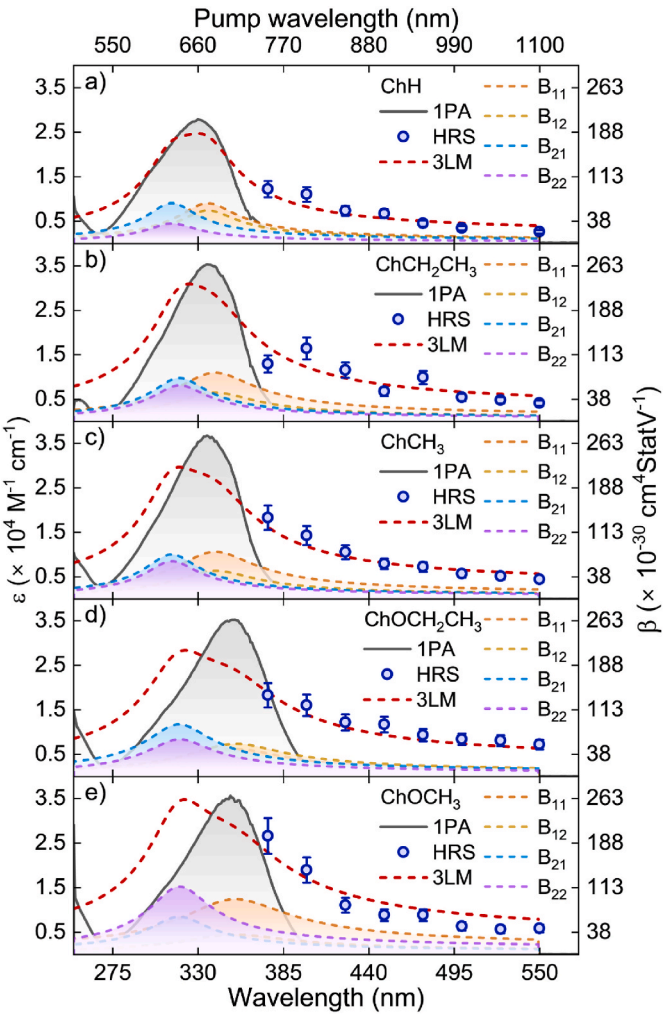

Fig. 6. – One-photon absorption (gray lines; right and bottom axes) and first-order molecular hyperpolarizability dispersion (blue circles; left and top axes) spectra for: a) **ChH**, b) **$ChCH_2CH_3$**, c) **$ChCH_3$**, d) **$ChOCH_2CH_3$**, and e) **$ChOCH_3$** in DMSO. Colored curves (orange, yellow, blue, and purple) represent the individual *n*LM terms B_{11}, B_{12}, B_{21}, and B_{22}, respectively, while the dark blue curve corresponds to the total superposition of these terms. (For interpretation of the references to colour in this figure legend, the reader is referred to the Web version of this article.)

Its optimal values are summarized in Table 2. It is important to highlight that the μ_{12} values obtained from the *n*LM are comparable, within the error, to those determined by the SOS model applied to the 2 PA spectra of the same compounds (see Table 2) [46]. In both cases, we employed the same photophysical parameters (μ_{0i}, $\Delta\mu_{0i}$, and ω_{0i}) and, a three-level system (one ground state and two excited states), keeping μ_{12} as the only free fitting parameter (spectral fitting range of $500 - 1000$ nm for the SOS model). This agreement arises because, although the models describe distinct nonlinear optical processes, both rely on the same molecular photophysical parameters, demonstrating the consistency of the adopted approach [18,19,41]. Further details on the model fitting and 2 PA spectra are available in Ref. [46].

Fig. 6 shows the dispersion of β (blue circles) fitted using the *n*LM (dashed red lines) over the $500 - 1100$ nm spectral window, with fit residuals varying within a relative range of $\pm 30 \times 10^{-30}$ cm^4 $StatV^{-1}$. In general, the model accurately describes the experimental data, yielding μ_{12} values between 3.0 and 7.5 D (see Table 2). Additionally, it is worth noting that Eqs. (2) and (3) exhibit a behavior in which the β value tends to increase as the wavelength gets shorter. This behavior arises from the dynamic terms of β, which present four resonance enhancement

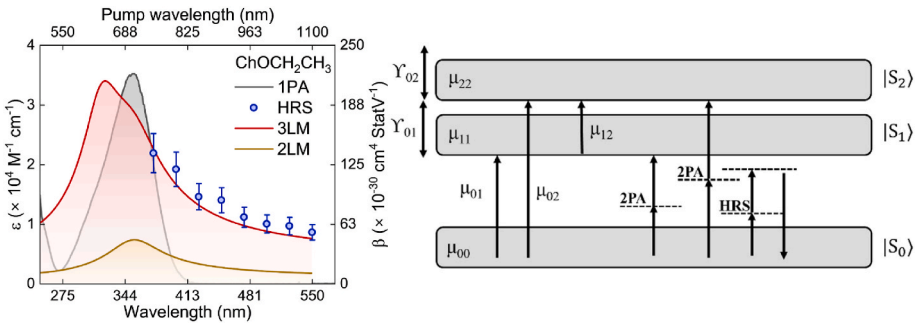

Fig. 7. – One-photon absorption (gray line; right and bottom axes) and first-order molecular hyperpolarizability dispersion (blue circles; left and top axes) spectrum for **ChOCH$_2$CH$_3$** in DMSO. The red and yellow curves correspond to the n-level model fit for three-level (3LM) and two-level (2LM) systems, respectively. The energy diagram illustrates the role of the photophysical parameters and the mechanisms of two-photon absorption and second-harmonic scattering. (For interpretation of the references to colour in this figure legend, the reader is referred to the Web version of this article.)

conditions in the denominators: two associated with one-photon resonances, $(\omega_{01} - \omega)$ and $(\omega_{02} - \omega)$, and two others related to two-photon resonances, $(\omega_{01} - 2\omega)$ and $(\omega_{02} - 2\omega)$. The former two conditions are negligible in our case, as the HRS measurements were performed outside the 1 PA region ($\lambda^{Pump} \geq 750\ nm$). However, the latter two terms become more significant for the magnitude of β in the $750 - 900\ nm$ spectral range. In this situation, the incident laser frequency is close to half the transition frequency of the first and second excited states, leading to a two-photon resonance enhancement ($\omega \approx \omega_{01}/2$ and $\omega \approx \omega_{02}/2$) in the β dispersion [18], as we discussed previously. Santos et al. [18] also discuss that this behavior implies that one-photon-allowed states are accessible via 2 PA as well, which requires non-zero $\Delta\mu_{0i}$ (see Table SI1); this characteristic is typical of molecules with low charge symmetry [17].

Another feature of the *n*LM is its capability to determine the minimum number of excited states required to describe the β spectrum. As previously mentioned, the molecules studied in this work exhibit two electronic excited states [46]; therefore, it is reasonable to employ the 3LM. However, one may question whether a simpler 2LM would already be sufficient to reproduce the experimental β dispersion. To test this assumption, we used only Eq. (3) to fit the β dispersion of the **ChOCH$_2$CH$_3$** molecule. It is worth noting that we maintained the same values of μ_{0i}, $\Delta\mu_{0i}$, ω_{0i}, and Υ_{0i} adopted in Eq. (2), ensuring consistency between the compared models.

As shown in Fig. 7 (yellow line), the 2LM does not adequately describe the experimental β dispersion, indicating the need to account for both electronic transitions to reproduce the molecular response. In this context, the B_{12}, B_{21}, and B_{22} terms associated with the second excited state contribute approximately 62% of the total β value at 750 *nm*. Another factor reinforcing the relevance of the second excited state is its proximity to the first one, which in this case is approximately 0.33 *eV*. For example, one can analyze the dynamic part of the B_{21} and B_{22} terms, which account for the two-photon resonance enhancement involving the second excited state $(\omega_{02} - 2\omega)$ (see blue and purple lines in Fig. 6). Due to the small energy difference between the two excited states, when the excitation wavelength approaches the lowest-energy transition, a two-photon resonant enhancement associated with the first excited state is observed, to which is added a non-negligible contribution from the second excited state, corresponding to 36% of the total β value at 750 *nm*. Finally, Fig. 7 presents an energy diagram that clearly illustrates the overall behavior of β dispersion observed for the acetamide-chalcone derivatives and the role of the photophysical parameters.

These findings demonstrate that our non-fluorescent acetamide-chalcone derivatives exhibit significant β values in the first near-infrared region (NIR-I: $700 - 900\ nm$), elucidating fundamental mechanisms and reinforcing their promising status as exogenous agents for ISHG microscopy in biological materials [3,4,7,9,25,59,60].

4. Conclusion

In this work, we investigated the effects of different ED groups on the β of five acetamide-chalcone derivatives, as well as their spectral dispersion. We obtained the β spectrum using the femtosecond laser-induced HRS technique in the $750 - 1100\ nm$ range, with a $50\ nm$ step size. The results showed that the **ChOCH$_3$** compound exhibits the highest $\beta_{\circ}$ value ($28 \times 10^{-30}\ cm^4\ stat\ V^{-1}$), indicating that, in our case, the –OCH$_3$ group plays a relevant role in enhancing the ISHG process, in agreement with previously reported literature data. Furthermore, the β spectra showed a pronounced increase for excitation wavelengths near a two-photon-allowed transition, with an enhancement of approximately 7 times the $\beta_{\circ}$ value. We also applied the *n*LM and compared it with the well-known SOS model. In both cases, we used the same photophysical parameters, and good agreement was observed for the μ_{12} values within the error. Thus, this work elucidates an efficient mechanism for optimizing β in acetamide-chalcone derivatives by combining appropriate molecular functionalization with the selection of the excitation spectral region.

Experimental details

The Supplementary Information provides a detailed table of the photophysical parameters used in the *n*-level model.

CRediT authorship contribution statement

André G. Pelosi: Data curation, Formal analysis, Investigation, Methodology, Writing – original draft. **João V.P. Valverde:** Data curation, Formal analysis, Investigation, Methodology, Writing – original draft, Writing – review & editing. **Carlos H. dos Santos:** Data curation, Formal analysis, Investigation, Methodology, Writing – original draft. **EliS.A. Ducas:** Formal analysis, Validation, Visualization, Writing – review & editing. **Pablo J. Gonçalves:** Formal analysis, Validation, Visualization, Writing – review & editing. **Cleber Renato Mendonça:** Funding acquisition, Supervision, Validation, Visualization, Writing – review & editing. **Leonardo De Boni:** Conceptualization, Funding acquisition, Project administration, Resources, Supervision, Validation, Visualization, Writing – original draft, Writing – review & editing.

Declaration of competing interest

The authors declare that they have no known competing financial interests or personal relationships that could have appeared to influence the work reported in this paper.

Acknowledgments

The authors acknowledge financial support from the São Paulo Research Foundation (FAPESP) under the grants 2025/01908-3 and 2018/11283-7. Conselho Nacional de Desenvolvimento Científico e Tecnológico (CNPq); Coordenação de Aperfeiçoamento de Pessoal de Nível Superior, Brasil (CAPES), Código de Financiamento 001; the Air Force Office of Scientific Research (AFOSR) (FA9550-23-1-0664); and the US Army (W911NF2110362).

Appendix A. Supplementary data

Supplementary data to this article can be found online at https://doi.org/10.1016/j.optmat.2026.117921.

Data availability

Data will be made available on request.

References

[1] A. Aghigh, S. Bancelin, M. Rivard, M. Pinsard, H. Ibrahim, F. Légaré, Second harmonic generation microscopy: a powerful tool for bio-imaging, Biophys. Rev. 15 (2023) 43–70, https://doi.org/10.1007/s12551-022-01041-6.

[2] P.J. Campagnola, H.A. Clark, W.A. Mohler, A. Lewis, L.M. Loew, Second-harmonic imaging microscopy of living cells, J. Biomed. Opt. 6 (2001) 277, https://doi.org/10.1117/1.1383294.

[3] P.J. Campagnola, M. Wei, A. Lewis, L.M. Loew, High-resolution nonlinear optical imaging of live cells by second harmonic generation, Biophys. J. 77 (1999) 3341–3349, https://doi.org/10.1016/S0006-3495(99)77165-1.

[4] J.E. Reeve, H.L. Anderson, K. Clays, Dyes for biological second harmonic generation imaging, Phys. Chem. Chem. Phys. 12 (2010) 13484, https://doi.org/10.1039/c003720f.

[5] J.E. Reeve, A.D. Corbett, I. Boczarow, W. Kaluza, W. Barford, H. Bayley, T. Wilson, H.L. Anderson, Porphyrins for probing electrical potential across lipid bilayer membranes by second harmonic generation, Angew. Chem. Int. Ed. 52 (2013) 9044–9048, https://doi.org/10.1002/anie.201304515.

[6] A.C. Millard, P.J. Campagnola, W. Mohler, A. Lewis, L.M. Loew, [3] second harmonic imaging microscopy, 47–69, https://doi.org/10.1016/S0076-6879(03)61005-0, 2003.

[7] X. Chen, O. Nadiarynkh, S. Plotnikov, P.J. Campagnola, Second harmonic generation microscopy for quantitative analysis of collagen fibrillar structure, Nat. Protoc. 7 (2012) 654–669, https://doi.org/10.1038/nprot.2012.009.

[8] E.E. Hoover, J.A. Squier, Advances in multiphoton microscopy technology, Nat. Photonics 7 (2013) 93–101, https://doi.org/10.1038/nphoton.2012.361.

[9] V. Van Steenbergen, W. Boesmans, Z. Li, Y. de Coene, K. Vints, P. Baatsen, I. Dewachter, M. Ameloot, K. Clays, P. Vanden Berghe, Molecular understanding of label-free second harmonic imaging of microtubules, Nat. Commun. 10 (2019) 3530, https://doi.org/10.1038/s41467-019-11463-8.

[10] S. Pascal, S. David, C. Andraud, O. Maury, Near-infrared dyes for two-photon absorption in the short-wavelength infrared: strategies towards optical power limiting, Chem. Soc. Rev. 50 (2021) 6613–6658, https://doi.org/10.1039/d0cs01221a.

[11] V. Alain, L. Thouin, M. Blanchard-Desce, U. Gubler, C. Bosshard, P. Günter, J. Muller, A. Fort, M. Barzoukas, Molecular engineering of push-pull phenylpolyenes for nonlinear optics: improved solubility, stability, and nonlinearities, Adv. Mater. 11 (1999) 1210–1214, https://doi.org/10.1002/(SICI)1521-4095(199910)11:14<1210::AID-ADMA1210>3.0.CO;2-R.

[12] H. Xu, D.L. Elder, L.E. Johnson, Y. de Coene, S.R. Hammond, W. Vander Ghinst, K. Clays, L.R. Dalton, B.H. Robinson, Electro-optic activity in excess of 1000 pm V −1 achieved via theory-guided organic chromophore design, Adv. Mater. 33 (2021), https://doi.org/10.1002/adma.202104174.

[13] J. Ma, S. Hu, X. Mu, R. Chen, K. Meng, B. Teng, L. Cao, D. Zhong, Structural design and characterization of a new chalcone molecular derivative crystal DMNC with high second-order nonlinear coefficient, Chin. J. Struct. Chem. 42 (2023) 100058, https://doi.org/10.1016/j.cjsc.2023.100058.

[14] E.L. DeWalt, V.J. Begue, J.A. Ronau, S.Z. Sullivan, C. Das, G.J. Simpson, Polarization-resolved second-harmonic generation microscopy as a method to visualize protein-crystal domains, Acta Crystallogr. D Biol. Crystallogr. 69 (2013) 74–81, https://doi.org/10.1107/S0907444912042503.

[15] S.J. Benight, D.H. Bale, B.C. Olbricht, L.R. Dalton, Organic electro-optics: understanding material structure/function relationships and device fabrication issues, J. Mater. Chem. 19 (2009) 7466, https://doi.org/10.1039/b905368a.

[16] L.R. Dalton, P.A. Sullivan, D.H. Bale, B.C. Olbricht, Theory-inspired nano-engineering of photonic and electronic materials: noncentrosymmetric charge-transfer electro-optic materials, Solid State Electron. 51 (2007) 1263–1277, https://doi.org/10.1016/j.sse.2007.06.022.

[17] M.G. Vivas, D.L. da Silva, C.R. Mendonca, L. De Boni, First-order hyperpolarizability of organic molecules: hyper-Rayleigh scattering and applications, in: Molecular and Laser Spectroscopy, Elsevier, 2020, pp. 275–314, https://doi.org/10.1016/B978-0-12-818870-5.00008-3.

[18] C.H.D. dos Santos, L.H. Zucolotto Cocca, A.G. Pelosi, V.F. Batista, D.C.G.A. Pinto, M.A.F. Faustino, M.G. Vivas, J. de Paula Siqueira, C.R. Mendonça, L. De Boni, Observation of the two-photon transition enhanced first hyperpolarizability spectra in cinnamaldehyde derivatives: a femtosecond regime study, J. Chem. Phys. 158 (2023) 214201, https://doi.org/10.1063/5.0151622.

[19] L.F. Sciuti, C.H.D. dos Santos, L.H.Z. Cocca, A.G. Pelosi, R.G.M. da Costa, J. Limberger, C.R. Mendonça, L. De Boni, Studying the first order hyperpolarizability spectra in chalcone-based derivatives and the relation with one- and two-photon absorption transitions, J. Chem. Phys. 159 (2023) 244311, https://doi.org/10.1063/5.0166036.

[20] S. Muhammad, A.G. Al-Sehemi, A. Irfan, A.R. Chaudhry, Tuning the push–pull configuration for efficient second-order nonlinear optical properties in some chalcone derivatives, J. Mol. Graph. Model. 68 (2016) 95–105, https://doi.org/10.1016/j.jmgm.2016.06.012.

[21] M.G. Vivas, D.L. Silva, R.D.F. Rodriguez, S. Canuto, J. Malinge, E. Ishow, C. R. Mendonca, L. De Boni, Interpreting the first-order electronic hyperpolarizability for a series of octupolar push–pull triarylamine molecules containing trifluoromethyl, J. Phys. Chem. C 119 (2015) 12589–12597, https://doi.org/10.1021/acs.jpcc.5b02386.

[22] S. Van Cleuvenbergen, I. Asselberghs, E.M. García-Frutos, B. Gómez-Lor, K. Clays, J. Pérez-Moreno, Dispersion overwhelms charge transfer in determining the magnitude of the first hyperpolarizability in triindole octupoles, J. Phys. Chem. C 116 (2012) 12312–12321, https://doi.org/10.1021/jp3022997.

[23] R.D. Fonseca, M.G. Vivas, D.L. Silva, G. Eucat, Y. Bretonnière, C. Andraud, L. De Boni, C.R. Mendonça, First-order hyperpolarizability of triphenylamine derivatives containing cyanopyridine: molecular branching effect, J. Phys. Chem. C 122 (2018) 1770–1778, https://doi.org/10.1021/acs.jpcc.7b05829.

[24] Y. Wu, Y. Li, Y. Zhang, B. Teng, X. Jiang, C. Hu, S. Sun, L. Cao, J. Ma, K. Xu, D. Xu, Z. Lin, D. Zhong, Toward the strongest nonlinear optical response and largest birefringence in solvent-free organic–inorganic metal halides by hydrogen bond engineering, Adv. Funct. Mater. 35 (2025), https://doi.org/10.1002/adfm.202503125.

[25] G. Hall, K.B. Tilbury, K.R. Campbell, K.W. Eliceiri, P.J. Campagnola, Experimental and simulation study of the wavelength dependent second harmonic generation of collagen in scattering tissues, Opt. Lett. 39 (2014) 1897, https://doi.org/10.1364/ol.39.001897.

[26] D.L. Silva, R.D. Fonseca, M.G. Vivas, E. Ishow, S. Canuto, C.R. Mendonca, L. De Boni, Experimental and theoretical investigation of the first-order hyperpolarizability of a class of triarylamine derivatives, J. Chem. Phys. 142 (2015) 064312, https://doi.org/10.1063/1.4906893.

[27] M.G. Vivas, C.A. Barboza, J.C. Germino, R.D. Fonseca, D.L. Silva, P.A.M. Vazquez, T.D.Z. Atvars, C.R. Mendonça, L. De Boni, Molecular structure–optical property relationship of salicylidene derivatives: a study on the first-order hyperpolarizability, J. Phys. Chem. A 125 (2021) 99–105, https://doi.org/10.1021/acs.jpca.0c08530.

[28] J.S. Dhaliwal, S. Moshawih, K.W. Goh, M.J. Loy, MdS. Hossain, A. Hermansyah, V. Kotra, N. Kifli, H.P. Goh, S.K.S. Dhaliwal, H. Yassin, L.C. Ming, Pharmacotherapeutics applications and chemistry of chalcone derivatives, Molecules 27 (2022) 7062, https://doi.org/10.3390/molecules27207062.

[29] M.A. Shalaby, S.A. Rizk, A.M. Fahim, Synthesis, reactions and application of chalcones: a systematic review, Org. Biomol. Chem. 21 (2023) 5317–5346, https://doi.org/10.1039/D3OB00792H.

[30] S. Narwal, B. Devi, T. Dhanda, S. Kumar, S. Tahlan, Exploring Chalcone derivatives: synthesis and their therapeutic potential, J. Mol. Struct. 1303 (2024) 137554, https://doi.org/10.1016/j.molstruc.2024.137554.

[31] L.F. Sciuti, L.M.G. Abegão, C.H.D. dos Santos, L.H. Zucolotto Cocca, R.G.M. da Costa, J. Limberger, L. Misoguti, C.R. Mendonça, L. De Boni, Modeling the first-order molecular hyperpolarizability dispersion from experimentally obtained One- and two-photon absorption, J. Phys. Chem. A 126 (2022) 2152–2159, https://doi.org/10.1021/acs.jpca.1c10559.

[32] J. Tan, Y. Zhang, M. Zhang, X. Tian, Y. Wang, S. Li, C. Wang, H. Zhou, J. Yang, Y. Tian, J. Wu, Small molecules of chalcone derivatives with high two-photon absorption activities in the near-IR region, J. Mater. Chem. C Mater. 4 (2016) 3256–3267, https://doi.org/10.1039/C6TC00382F.

[33] S.-C. Lee, N.-Y. Kang, S.-J. Park, S.-W. Yun, Y. Chandran, Y.-T. Chang, Development of a fluorescent chalcone library and its application in the discovery of a mouse embryonic stem cell probe, Chem. Commun. 48 (2012) 6681, https://doi.org/10.1039/c2cc31662e.

[34] P. Li, R. Li, K. Wang, Q. Liu, B. Ren, Y. Ding, R. Guan, D. Cao, A julolidine-chalcone-based fluorescent probe for detection of Al3+ in real water sample and cell imaging, Spectrochim. Acta Mol. Biomol. Spectrosc. 276 (2022) 121213, https://doi.org/10.1016/j.saa.2022.121213.

[35] S. Wangngae, T. Pewklang, K. Chansaenpak, P. Ganta, S. Worakaensai, K. Siwawannapong, S. Kluaiphanngam, N. Nantapong, R.-Y. Lai, A. Kamkaew, A chalcone-based fluorescent responsive probe for selective detection of nitroreductase activity in bacteria, New J. Chem. 45 (2021) 11566–11573, https://doi.org/10.1039/D1NJ01794B.

[36] S. Wangngae, K. Chansaenpak, J. Nootem, U. Ngivprom, S. Aryamueang, R.-Y. Lai, A. Kamkaew, Photophysical study and biological applications of synthetic chalcone-based fluorescent dyes, Molecules 26 (2021) 2979, https://doi.org/10.3390/molecules26102979.

[37] P. Kumar, R. Singh, D. Sharma, Q.P. Hassan, B. Gopu, J.M.H. Anal, Design, synthesis, and biological evaluation of chalcone acetamide derivatives against

triple negative breast cancer, Bioorg. Med. Chem. Lett. 107 (2024) 129795, https://doi.org/10.1016/j.bmcl.2024.129795.
[38] O. Alshazly, G.E.-D.A. Abuo-Rahma, M.F.A. Mohamed, M. Abdel-Aziz, Amide linked chalcone derivatives, a promising class of compounds with versatile biological effects, RSC Adv. 15 (2025) 19043–19068, https://doi.org/10.1039/D5RA00834D.
[39] C. Zhuang, W. Zhang, C. Sheng, W. Zhang, C. Xing, Z. Miao, Chalcone: a privileged structure in medicinal chemistry, Chem. Rev. 117 (2017) 7762–7810, https://doi.org/10.1021/acs.chemrev.7b00020.
[40] J. Dong, Y. Wang, C. Fan, Y. Tu, S. Pu, Chalcone dye-based fluorescent probe for selective and specific detection of cysteine in lysosomes of living cells, Dyes Pigments 210 (2023) 110994, https://doi.org/10.1016/j.dyepig.2022.110994.
[41] L.F. Sciuti, L.M.G. Abegão, C.H.D. Dos Santos, L.H. Zucolotto Cocca, R.G.M. Da Costa, J. Limberger, L. Misoguti, C.R. Mendonça, L. De Boni, Modeling the first-order molecular hyperpolarizability dispersion from experimentally obtained One- and two-photon absorption, J. Phys. Chem. A 126 (2022) 2152–2159, https://doi.org/10.1021/acs.jpca.1c10559.
[42] N.B. Marucci, J.V.P. Valverde, G. de O. Campos, E.S.A. Ducas, P.J. Gonçalves, L. De Boni, C.R. Mendonça, Two-Photon absorption and dynamics of excited states in bromochalcone derivatives, J. Phys. Chem. A 129 (2025) 9119–9128, https://doi.org/10.1021/acs.jpca.5c02748.
[43] D. Hadji, T. Bensafi, B. Baroudi, Chalcone derivatives with strong nonlinear optical activity, J. Opt. 54 (2025) 2227–2246, https://doi.org/10.1007/s12596-024-01931-w.
[44] A. Benmohammed, D. Hadji, Y. Mouchaal, A. Djafri, Synthesis and characterization of novel chalcone with good nonlinear optical properties, Chem. Afr. 8 (2025) 85–97, https://doi.org/10.1007/s42250-024-01143-6.
[45] L.M.G. Abegão, F.A. Santos, R.D. Fonseca, A.L.B.S. Barreiros, M.L. Barreiros, P. B. Alves, E.V. Costa, G.B. Souza, M.A.R.C. Alencar, C.R. Mendonça, K. Kamada, L. De Boni, J.J. Rodrigues, Chalcone-based molecules: experimental and theoretical studies on the two-photon absorption and molecular first hyperpolarizability, Spectrochim. Acta Mol. Biomol. Spectrosc. 227 (2020) 117772, https://doi.org/10.1016/j.saa.2019.117772.
[46] A.G. Pelosi, E. Silveira-Alves, L.H.Z. Cocca, J.V. Valverde, G.R. Oliveira, D.L. da Silva, L. De Boni, P.J. Gonçalves, C.R. Mendonca, Two-Photon absorption and multiphoton excited fluorescence of acetamide-chalcone derivatives: the role of dimethylamine group on the nonlinear optical and photophysical properties, Molecules 28 (2023) 1572, https://doi.org/10.3390/molecules28041572.
[47] K. Clays, A. Persoons, Hyper-rayleigh scattering in solution, Rev. Sci. Instrum. 63 (1992) 3285–3289, https://doi.org/10.1063/1.1142538.
[48] K. Clays, A. Persoons, Hyper-rayleigh scattering in solution with tunable femtosecond continuous-wave laser source, Rev. Sci. Instrum. 65 (1994) 2190–2194, https://doi.org/10.1063/1.1144725.
[49] K. Clays, A. Persoons, Hyper-rayleigh scattering in solution, Phys. Rev. Lett. 66 (1991) 2980–2983, https://doi.org/10.1103/PhysRevLett.66.2980.
[50] J. Campo, W. Wenseleers, E. Goovaerts, M. Szablewski, G.H. Cross, Accurate determination and modeling of the dispersion of the first hyperpolarizability of an efficient zwitterionic nonlinear optical chromophore by tunable wavelength hyper-rayleigh scattering, J. Phys. Chem. C 112 (2008) 287–296, https://doi.org/10.1021/jp0758824.
[51] M.A. Pauley, H.-W. Guan, C.H. Wang, A.K.-Y. Jen, Determination of first hyperpolarizability of nonlinear optical chromophores by second harmonic scattering using an external reference, J. Chem. Phys. 104 (1996) 7821–7829, https://doi.org/10.1063/1.471669.
[52] R.D. Fonseca, M.G. Vivas, D.L. Silva, G. Eucat, Y. Bretonnière, C. Andraud, L. De Boni, C.R. Mendonça, First-order hyperpolarizability of triphenylamine derivatives containing cyanopyridine: molecular branching effect, J. Phys. Chem. C 122 (2018) 1770–1778, https://doi.org/10.1021/acs.jpcc.7b05829.
[53] Corwin Hansch, A. Leo, R.W. Taft, A survey of Hammett substituent constants and resonance and field parameters, Chem. Rev. 91 (1991) 165–195, https://doi.org/10.1021/cr00002a004.
[54] A. Kenane, D. Hadji, K. Argoub, A. Yahiaoui, A. Hachemaoui, K. Toubal, A. M. Benkouider, O. Rasoga, A. Stanculescu, A. Galca, Efficient NLO materials based on Poly(ortho-anisidine) and polyaniline: a quantum chemical study, J. Electron. Mater. 52 (2023) 530–539, https://doi.org/10.1007/s11664-022-10022-0.
[55] H. Djebar, B. Toufik, B. Benamar, Analyzing structure–nonlinear optical relationships in phenols, J. Electron. Mater. 54 (2025) 2980–3000, https://doi.org/10.1007/s11664-025-11785-y.
[56] D. Hadji, A. Benmohammed, Y. Mouchaal, A. Djafri, Synthesis and characterization of novel thiosemicarbazide for nonlinear optical applications: combined experimental and theoretical study, Rev. Roum. Chem. 68 (2023) 463–471, https://doi.org/10.33224/rrch.2023.68.9.07.
[57] L.M.G. Abegão, R.D. Fonseca, F.A. Santos, G.B. Souza, A.L.B.S. Barreiros, M. L. Barreiros, M.A.R.C. Alencar, C.R. Mendonça, D.L. Silva, L. De Boni, J. J. Rodrigues, Second- and third-order nonlinear optical properties of unsubstituted and mono-substituted chalcones, Chem. Phys. Lett. 648 (2016) 91–96, https://doi.org/10.1016/j.cplett.2016.02.009.
[58] W. Bartkowiak, R. Zaleśny, J. Leszczynski, Relation between bond-length alternation and two-photon absorption of a push–pull conjugated molecules: a quantum-chemical study, Chem. Phys. 287 (2003) 103–112, https://doi.org/10.1016/S0301-0104(02)00982-5.
[59] N. Kato, Optical second harmonic generation microscopy: application to the sensitive detection of cell membrane damage, Biophys. Rev. 11 (2019) 399–408, https://doi.org/10.1007/s12551-019-00546-x.
[60] V.V. Dudenkova, M.V. Shirmanova, M.M. Lukina, F.I. Feldshtein, A. Virkin, E. V. Zagainova, Examination of collagen structure and state by the second harmonic generation microscopy, Biochemistry (Mosc.) 84 (2019) 89–107, https://doi.org/10.1134/S0006297919140062.